

## Article

# Investigating Effect of Pumping Ratio on Effectiveness of Barrier Wells for Saltwater Intrusion: Lab-Scale Experiments and Numerical Modeling

Shinichi Ozaki <sup>1</sup>, Christel Abi Akl <sup>2</sup>, Tatsuya Nagino <sup>2</sup> and Yoshinari Hiroshiro <sup>2,\*</sup><sup>1</sup> Nippon Koei Co., Ltd., 5-4, Koji-Machi, Chiyoda-Ku, Tokyo 102-8539, Japan; sinlog5296@gmail.com<sup>2</sup> Urban and Environmental Engineering, Graduate School of Engineering, Kyushu University, 744 Motoooka, Nishi-ku, Fukuoka 819-0395, Japan; christelaa31@gmail.com (C.A.A.); rincoon.0127@gmail.com (T.N.)

\* Correspondence: hiroshiro@civil.kyushu-u.ac.jp; Tel.: +81-92-802-3430

**Abstract:** Saltwater intrusion, leading to the salinization of fresh groundwater, is the most challenging problem in coastal regions. Saltwater pumping from a barrier well is widely applied to prevent saltwater intrusion. Owing to its easy installation, many studies have investigated saltwater pumping. However, quantitative relationships between the barrier and inland production wells have not been revealed. In this study, lab-scale experiments were conducted to examine the effectiveness of a barrier well on the possible flow rate of freshwater from a production well. Moreover, a two-dimensional numerical model was created and simulated under the same conditions as those used in the experiments to analyze the experimental results. Consequently, a critical pumping ratio of 1.9 was obtained. In the numerical simulation, it was confirmed that an upconing of highly concentrated saltwater toward the barrier well was observed when the pumping ratio was less than the critical ratio. In conclusion, there is a critical pumping ratio between the barrier and the production well, and saltwater intrusion can be controlled by keeping the pumping rates under the critical ratio. Although further studies have yet to be conducted on a practical scale, this study showed the potential of the pumping ratio control to manage saltwater intrusion.

**Keywords:** salinity-affected coastal aquifer; saltwater intrusion; barrier well; production well; critical groundwater pumping ratio; laboratory experiment; global warming; sandy aquifer



**Citation:** Ozaki, S.; Akl, C.A.; Nagino, T.; Hiroshiro, Y. Investigating Effect of Pumping Ratio on Effectiveness of Barrier Wells for Saltwater Intrusion: Lab-Scale Experiments and Numerical Modeling. *Water* **2021**, *13*, 2100. <https://doi.org/10.3390/w13152100>

Academic Editor: Giuseppe Sappa

Received: 30 April 2021

Accepted: 29 July 2021

Published: 31 July 2021

**Publisher's Note:** MDPI stays neutral with regard to jurisdictional claims in published maps and institutional affiliations.



**Copyright:** © 2021 by the authors. Licensee MDPI, Basel, Switzerland. This article is an open access article distributed under the terms and conditions of the Creative Commons Attribution (CC BY) license (<https://creativecommons.org/licenses/by/4.0/>).

## 1. Introduction

Saltwater intrusion is the lateral encroachment of seawater toward the coastal aquifer, leading to the salinization of groundwater and reduction in available freshwater sources. It is the most challenging problem in coastal regions. Saltwater intrusion is known to contaminate significantly large areas, spanning several kilometers in some cases [1]. According to Sherif et al. [2], seawater intrusion has reached more than 100 km away from the coast in the Nile Delta aquifer, Egypt, even though it is perhaps the only case that seawater has intruded more than 100 km. Once contaminated, the area requires long-term management to be restored to its initial condition [3]. Ebeling et al. [4] showed that it can take as long as decades or centuries to remediate saltwater intrusion even with a mixed hydraulic barrier. Although saltwater intrusion is naturally caused due to the density difference between saltwater and freshwater, external factors resulting from human activities cause saltwater intrusion to advance further inland. Concentrated populations in coastal regions result in increased demand for potable water and accelerated groundwater pumping, leading to groundwater depletion, especially in arid and semi-arid regions [5]. Moreover, the rise in seawater level associated with global warming and climate change is regarded as the most influential factor on saltwater intrusion in the future [6]. It was reported by FAO [7] that an increase in sea level migrates the mixing zone of freshwater and saltwater in coastal aquifers toward the inland. In fact, Sherif et al. [8] revealed that 0.5 m of sea

level rise would cause 9.0 km and 0.4 km of additional seawater intrusion in the Nile Delta aquifer in Egypt and the Madras aquifer in India without any countermeasures, respectively. Abd-Elhamid et al. [1] also simulated the effects of seawater rise and over pumping on seawater intrusion in the Gaza aquifer, Palestine, using a 2D-FEST model. This simulation showed that 1.0 m of sea level rise and 0.5 m of head loss on the land side can cause 500 m and 250 m of further intrusion into the aquifer, respectively, and the combination of the sea level rise and GW head loss can cause 1000 m of further intrusion. The IPCC's Fifth Assessment Report [9] predicts that sea level will rise in more than 95% of the ocean areas on earth, with an 82 cm average rise between 2006 and 2100. This will lead to an increase in the level of the salt–freshwater interface, which will further advance groundwater salinization inland.

Various countermeasures have been developed to prevent saltwater intrusion. They are primarily categorized into three different groups: conventional methods, physical barriers, and hydraulic barriers [10]. Among these countermeasures, a negative hydraulic barrier using barrier wells pumping saline or brackish water is widely used (Figure 1). The extracted water can be directly discharged into the sea or used as a water source for desalination plants. Stein et al. [11] demonstrated that this method can provide an alternative water source for desalination plants, as well as remediate saltwater intrusion, while simultaneously pumping freshwater inland for domestic or industrial use. Besides, this method has a good applicability, as it does not need any other water source for the application, and existing wells can also be utilized as a barrier well. Considering these advantages, many studies have investigated the saltwater pumping process.

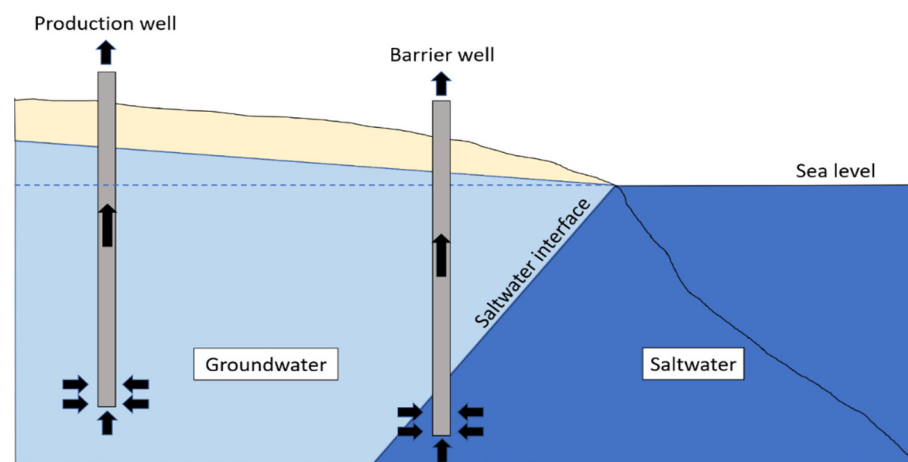


**Figure 1.** Conceptual diagram of saltwater pumping by a barrier well.

Vat et al. [12] revealed the effectiveness of a groundwater circulation well as a countermeasure to seawater intrusion with a lab-scale experiment and a numerical simulation using FEMWATER. In their study, the behavior of seawater intrusion dynamics was investigated using an experimental setup simulating a coastal unconfined aquifer with glass beads and saltwater colored by red food coloring, which is often used for lab-scale experiments simulating groundwater environments. Sherif and Hamza [13] numerically analyzed the relationship between the position of the barrier well and the behavior of saltwater intrusion, leading to a significant reduction in the width of the mixing zone due to brackish water pumping. Moreover, some studies have analyzed a dual pumping system composed of a barrier well for saltwater pumping and a production well for freshwater pumping. Pool and Carrera [14] used a three-dimensional variable-density flow model to study the dynamics of this system. They demonstrated that this model would have high efficiency in shallow aquifers, and its efficiency would even increase in cases where the seawater pumps saline water at high rates in a zone close to the sea. Park et al. [15] numerically analyzed the effects of different parameters, including the positions, pumping rates, and number of

barrier wells, on the quality of water pumped from another production well. The highest efficiency was obtained when a single barrier well was located in the middle of the coastline and the production well extracts saltwater at a rate that is 30% of the freshwater pumping rate from a production well. Although these studies demonstrated a good performance of the dual pumping system, the limit of the possible flow rate from the production well was not clarified. If the possible flow rate can be determined by the pumping ratio between the barrier and production well, saltwater intrusion can be controlled by manipulating the water ratio, which can be implemented in any salinized coastal area. Therefore, fundamental research that considers the effectiveness of barrier wells in relation to possible water pumping from production wells is necessary. In this study, basic lab-scale experiments and numerical simulations were conducted to examine the effect of saltwater pumping on possible freshwater pumping from an inland production well.

## 2. Methodology

### 2.1. Lab-Scale Experiments

The experimental device used was a transparent acrylic water tank with an internal length, height, and width of 122.1, 40.0, and 10.6 cm, respectively (Figure 2). It consisted of a freshwater tank on the far right, a permeation tank in the center, and a saltwater tank on the far left. Storage tanks for saltwater and freshwater were installed on both sides, and overflow drainage was provided at adjustable heights to control the water head in both tanks. Freshwater and saltwater were supplied to these storage tanks by pumps that maintained constant heads of saltwater and freshwater of 30.0 cm and 31.5 cm, respectively. The central chamber was lined with a  $5 \times 5$  cm grid to enable direct measurement of the positions and shapes of the saltwater intrusion. The permeation tank was evenly filled with glass beads (ASGB-20 made by AS ONE) to a height of 31.5 cm under saturated conditions to minimize the entrapment of air into the device. The glass beads, which were selected based on their sizes and porosities, represented sand in a sandy coastal unconfined aquifer. The particle sizes of the glass beads ranged from 0.71 to 1.00 mm, which corresponded to the range of coarse sand in the Wentworth grain-size classification [16]. Moreover, the porosity of the glass beads was calculated from the mass and volume of the glass beads and the amount of freshwater injected (34.8%) when the glass beads were placed. According to the porosity classification of the deposits, the porosity was within the range of sand porosity [17]. Two wells, A and B, were installed in the permeation tank. Well A represented the barrier well for pumping saltwater, and Well B represented the production well for pumping fresh groundwater. They were located at 50 and 75 cm from the left end of the saltwater tank, respectively; their heights were the same, that is, 15 cm from the bottom of the permeation tank. Both wells had valves to control the quantity of water being pumped. The freshwater used was from university tap water, and its density was measured to be  $0.991 \text{ g/cm}^3$ . Saltwater was prepared by adding commercial salt to tap water to achieve a density of  $1.025 \text{ g/cm}^3$ , which corresponded to seawater density [18,19]. Additionally, saltwater was dyed red using food coloring to observe the salt–freshwater interface. Hydraulic conductivity was calculated in each experiment using the measured flow rates and the assumption of the Dupuit–Fawer equations [20]. However, the calculated values of hydraulic conductivity changed through repeated experiments. This difference was caused by the bulge of the acrylic plates on the sides of the experimental device due to the settling of glass beads.

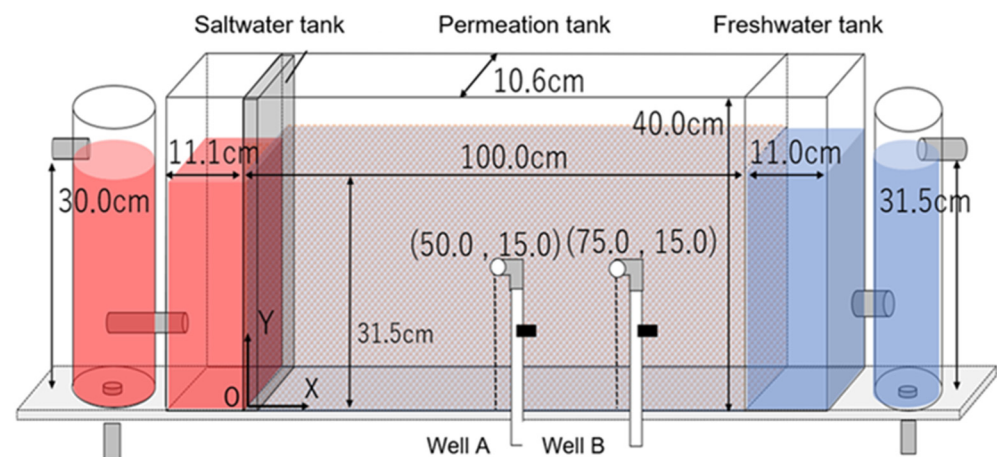


**Figure 2.** Conceptual diagram of the experimental device. (Well A is a barrier well and Well B is a production well.)

The experiment consisted of five steps (Figure 3). When the steady state was achieved in the ongoing step, the experiment was moved to the next step. The experiment continued until all steps were completed; the process was recorded using a digital camera. Step 1 represents the formation of a saltwater wedge because of the head differences between fresh and salt water. In Step 2, water was pumped from Well A, and the advancement of the salt–freshwater interface was observed for different water pumping rates. This was followed by Step 3, in which water was pumped simultaneously from Wells A and B. Further advancement of the salt–freshwater interface was observed at this stage and compared to the respective pumping ratios in each experiment. Step 4 began when pumping from Well B was turned off, resulting in the saltwater intrusion retreating to the steady-state position that was achieved in Step 2. Step 5 began when pumping from Well A was turned off; thus, no more water was pumped from the experimental device. The saltwater intrusion retracted to the position of the steady state achieved in Step 1. One full experiment, including all five steps, was performed six times with different pumping ratios to ensure that comparative considerations can be carried out on test results to consider the positive effect of preventing salinization by pumping saltwater from the barrier well. The experimental parameters, including hydraulic conductivities, pumping rates from wells A and B, and pumping ratios are presented in Table 1.

**Table 1.** Experimental parameters. Hydraulic conductivities, pumping rates at Wells A and B, and pumping ratios.

Experiment No.	1	2	3	4	5	6
Hydraulic conductivity (cm/s)	0.45	0.40	0.53	0.50	0.39	0.48
Water intake at point A; $Q_A$ (mL/s)	1.8	2.9	2.5	2.7	2.7	2.2
Water intake at point B; $Q_B$ (mL/s)	1.7	3.5	3.8	5.2	5.3	5.7
Water intake ratio; $Q_B/Q_A$	0.9	1.2	1.5	1.9	2.0	2.6

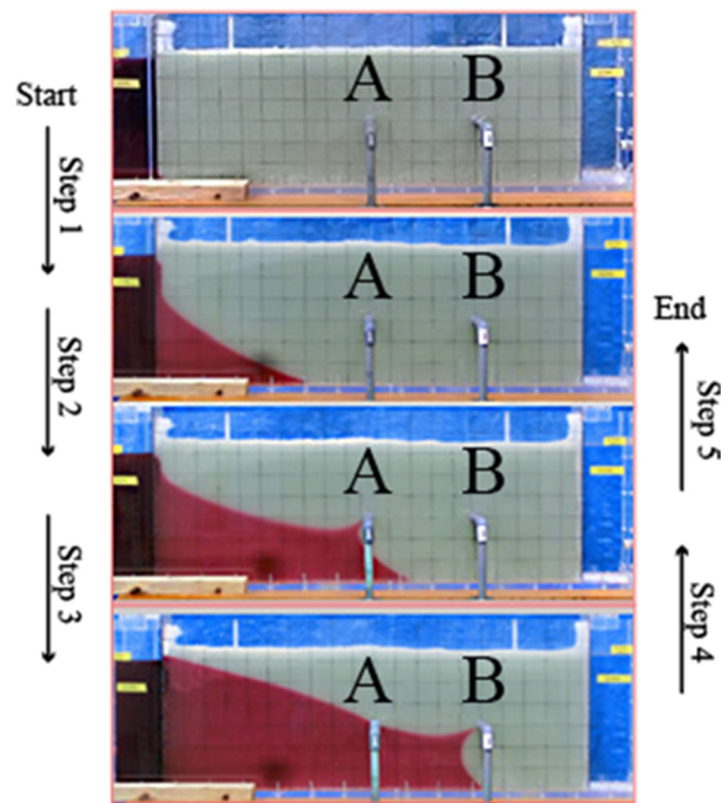


**Figure 3.** Experimental procedure, showing the intrusion process for pumping ratio of 2.6 as an example.

## 2.2. Numerical Model

A numerical simulation was conducted to analyze the results obtained from lab-scale experiments with different hydraulic conductivities and pumping rates of the barrier well and production well. A two-dimensional density-dependent solute transport model was used as the mathematical model in this study. The model was composed of the groundwater flow equation and solute transport equation for advection and dispersion transport.

The groundwater flow equations for the potential head in saturated–unsaturated aquifers can be described as follows:

$$(C_w + \alpha_0 S) \frac{\partial h}{\partial t} = -\frac{\partial u}{\partial x} - \frac{\partial v}{\partial y} \quad (1)$$

$$u = -k \frac{\partial h}{\partial x} \quad (2)$$

$$v = -k \left( \frac{\partial h}{\partial y} + \frac{\rho}{\rho_f} \right) \quad (3)$$

where  $t$  is the time period;  $h$  is the potential head;  $k$  is the hydraulic conductivity;  $u$  and  $v$  are the Darcy velocities in the  $x$ - and  $y$ -directions, respectively;  $\rho$  is the fluid density;  $\rho_f$  is the density of freshwater;  $C_w$  is the specific moisture capacity;  $S$  is the specific storage coefficient;  $\alpha$  is a dummy parameter that takes 0 in the unsaturated condition and 1 in the saturated condition. The specific storage coefficient represents the amount of water stored in the soil per unit volume when the hydraulic head in the unit is raised. It is known that the specific storage coefficient ranges from  $10^{-1}$  to  $10^{-2}$   $\text{cm}^{-1}$  in unconfined aquifers and  $10^{-6}$  to  $10^{-7}$   $\text{cm}^{-1}$  in confined aquifers [21].

With the volumetric water content  $\theta$ , the specific moisture capacity is defined as

$$C_w = \frac{d\theta}{dh} \quad (4)$$

In the saturated zone, the specific moisture capacity is equal to 0.

This model can calculate the pressure head for both saturated and unsaturated zones. To calculate the unsaturated zone flow, unsaturated flow parameters such as the volumetric water content ( $\theta$ ), ratio of saturated hydraulic conductivity ( $k_s$ ), unsaturated hydraulic conductivity ( $k$ ), and specific moisture capacity ( $C_w$ ) are required. However, these parameters have not been examined in lab-scale experiments. Therefore, the following formulas for unsaturated flow parameters suggested by van Genuchten [22] were used: using these formulas, the relationship between the negative pressure head and the unsaturated flow parameters mentioned above was obtained.

$$Se = \frac{\theta - \theta_r}{\theta_s - \theta_r}, \quad Se = \left[ \frac{1}{1 + (\alpha|h|)^n} \right]^m \quad (5)$$

$$k_r = Se^{\frac{1}{2}} \left\{ 1 - \left( 1 - Se^{\frac{1}{m}} \right)^m \right\}^2 \quad (6)$$

$$C_w = \frac{\alpha \cdot m (\theta_s - \theta) Se^{\frac{1}{m}} \left( 1 - Se^{\frac{1}{m}} \right)^m}{1 - m} \quad (7)$$

where  $\theta_r$  is the residual water content,  $\theta_s$  is the saturated water content, and  $\alpha$ ,  $m$ , and  $n$  are the coefficients of the van Genuchten formula. Referring to Jinno et al. [23], these parameters were determined and are presented in Table 2.

**Table 2.** Parameters for van Genuchten formula.

<b>Saturated water content</b>		0.342
<b>Residual water content</b>		0.075
<b>Coefficient</b>	<b><math>\alpha</math></b>	0.0491 (cm/s)
	<b><math>m</math></b>	0.8599
	<b><math>n</math></b>	7.138

In two-dimensional transient groundwater systems, the fundamental equation for the solute concentration can be written as:

$$\begin{aligned} & \frac{\partial(\theta C)}{\partial t} + \frac{\partial(u'\theta C)}{\partial x} + \frac{\partial(v'\theta C)}{\partial y} \\ & = \frac{\partial}{\partial x} \left( \theta D_{xx} \frac{\partial C}{\partial x} + \theta D_{xy} \frac{\partial C}{\partial y} \right) + \frac{\partial}{\partial y} \left( \theta D_{yy} \frac{\partial C}{\partial y} + \theta D_{yx} \frac{\partial C}{\partial x} \right) \end{aligned} \quad (8)$$

where  $C$  is the solute concentration,  $\theta$  is the volumetric water content, and  $u'$  and  $v'$  are the actual pore velocities in the  $x$ - and  $y$ -directions, respectively. Using Darcy's velocity,  $u'$  and  $v'$  are described as:

$$u' = \frac{u}{\theta}, \quad v' = \frac{v}{\theta} \quad (9)$$

The products of the volumetric water content and dispersion coefficient,  $\theta D_{xx}$ ,  $\theta D_{xy}$ ,  $\theta D_{yx}$ , and  $\theta D_{yy}$ , are expressed as

$$\theta D_{xx} = \frac{\alpha_L u^2}{V} + \frac{\alpha_T v^2}{V} + \theta D \quad (10)$$

$$\theta D_{yy} = \frac{\alpha_T u^2}{V} + \frac{\alpha_L v^2}{V} + \theta D_M \quad (11)$$

$$\theta D_{xy} = \theta D_{yx} = \frac{(\alpha_L - \alpha_T)uv}{V} \quad (12)$$

$V$  is the magnitude of the velocity vector, which is written as:

$$V = (u^2 + v^2)^{\frac{1}{2}} \quad (13)$$

where  $D_{xx}$  and  $D_{yy}$  are the principal components of the dispersion tensor,  $D_{xy}$  and  $D_{yx}$  are the cross-terms of the dispersion tensor,  $\alpha_L$  and  $\alpha_T$  are the longitudinal dispersion length and the transverse dispersion length, respectively, and  $D_M$  is the molecular diffusion coefficient. When the velocity vector is aligned with one of the coordinate axes, all the cross-terms become zero.

The relationship between the salt concentration of water and fluid densities was calculated as follows [24]:

$$C = \frac{\rho - \rho_f}{\rho_s - \rho_f} \times 100(\%) \quad (14)$$

where  $C$  is the salt concentration of water in the flow domain, and  $\rho_f$  and  $\rho_s$  are the densities of freshwater and saltwater, respectively.

The mathematical solution used to solve the above equations is based on the finite difference method. In addition, under the groundwater flow condition of this study, a partial change in the velocity distribution in the mixing zone of saltwater and freshwater was expected, requiring an accurate numerical solution to calculate the concentration flux caused by advection. To solve this problem, the method of characteristics was applied [21]. The method of characteristics was developed using a conventional partial tracking technique. Particles were randomly or regularly distributed in the model field. Each particle is associated with its concentration and coordinates. These particles are exposed to the flow and transported from the initial positions by the flow in each time increment. Tracking the positions of particles within every time increment, the concentrations of particles located in a target cell were recorded, and the mean concentration among the recorded concentrations was evaluated as the concentration at the cell. The advantage of this method is that the accuracy and stability of the solution are high when the advection domains are in the flow rather than the dispersion.

The grid sizes and the time increment for the simulation were determined by considering the conditions of the lab-scale experiments. The model domain for the solute transport model was divided with a grid length of 0.5 cm each in the x- and y-directions. The time increment was set to be 0.5 s to meet the stability condition of the model. Other parameters for the simulation need to be determined from the available information. Hydraulic parameters, including the hydraulic conductivity, saltwater and freshwater densities, porosity of the glass beads, and volumetric water content, for the simulation were obtained from the experiments. Moreover, the longitudinal dispersion length and transverse dispersion length were calculated using the following formulas reported by Harleman and Rumer [25]:

$$\frac{D_L}{v} = 0.66 \left( \frac{q'^{d_m}}{v} \right)^{1.2} = \frac{\alpha_L q'}{v} \quad (15)$$

$$\frac{D_T}{v} = 0.036 \left( \frac{q'^{d_m}}{v} \right)^{0.72} = \frac{\alpha_T q'}{v} \quad (16)$$

where  $D_L$  and  $D_T$  are longitudinal and transverse dispersion coefficients, respectively, and  $q'$  is the flow rate per unit width in the aquifer.

The above equations are valid when the Reynolds number ranges from 0.05 to 3.5. In this study, the Reynolds number was calculated to be 0.17; therefore, the above equations can be applied for longitudinal and transverse dispersion lengths. The numerical and hydrological parameters used are listed in Table 3. The model boundaries are defined as

shown in Figure 4. Table 4 lists the boundary conditions of each boundary. The model consisted of six boundaries: the top surface of saltwater (AE), top surface of freshwater (ED), bottom surface (BC), saltwater boundary (EF), and two vertical boundaries (AB and CD). For the bottom surface, no discharge flow boundary was assigned. The other boundaries were assigned with time-dependent pressure head boundaries that varied with the water table heights of the boundaries. The concentrations at the boundaries were defined as zero at the right vertical boundary and 100% at the left vertical boundary. For the top and bottom boundaries, the concentration gradient was zero. In the numerical simulation, the hydraulic conductivity and pumping rates from the barrier and production wells were changed in each case, as well as in the lab-scale experiments, to run the model under the same conditions as the experiments. Therefore, the hydraulic conductivity, the pumping rates at the barrier and production wells, and the pumping ratio between the barrier and production wells were decided to be the same as the experiments as shown in Table 1. The numerical model was coded in the FORTRAN programming language and run using Microsoft Visual Studio 2008. The validity of this model was confirmed by visually comparing the simulated and experimental results for each step.

**Table 3.** Numerical and hydrological parameters for simulation.

Time Interval	$\Delta t$	0.5 (s)
Cell length in x direction	$\Delta x$	0.5 (cm)
Cell length in y direction	$\Delta y$	0.5 (cm)
Longitudinal dispersion length	$\alpha_L$	0.038 (cm)
Transverse dispersion length	$\alpha_T$	0.0051 (cm)
Molecular diffusion	$D_M$	$1.0 \times 10^{-5}$ (cm <sup>2</sup> /s)
Porosity	$n_e$	0.35
Freshwater head	$H_f$	31.5 (cm)
Saltwater head	$H_s$	30.0 (cm)
Freshwater density	$\rho_s$	0.991 (g/cm <sup>3</sup> )
Saltwater density	$\rho_f$	1.025 (g/cm <sup>3</sup> )
Extrapolation factor for SOR method	$\omega$	1.6
Criteria for convergence judgement	$\epsilon_0$	$1.0 \times 10^{-2}$
Specific storage coefficient	$S_S$	0.1

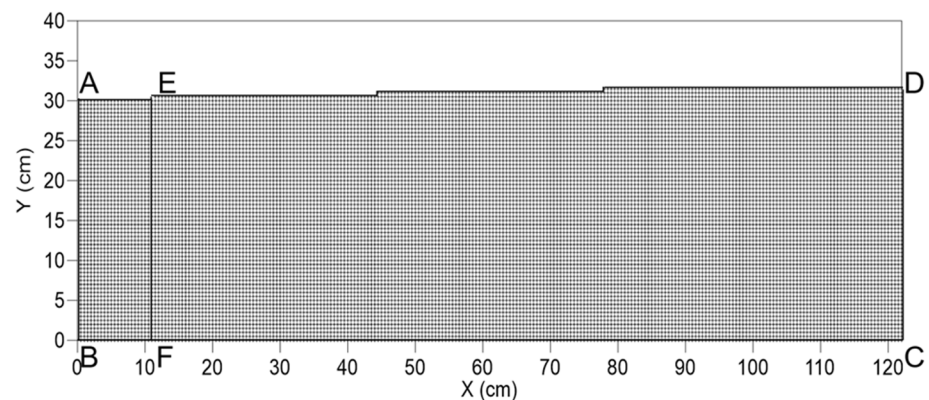


**Figure 4.** Numerical model and boundaries.

**Table 4.** Boundary conditions.

Boundary	Pressure Head	Conc.
AB	$h = (H_s - y) \frac{\rho_s}{\rho_f}$	$C = 100\%$
BC	$-k \left( \frac{\partial h}{\partial y} + \frac{\rho}{\rho_f} \right) = 0$	$\frac{\partial C}{\partial y} = 0$
CD	$h = (H_s - y)$	$C = 0\%$
DE	$-k \left( \frac{\partial h}{\partial y} + \frac{\rho}{\rho_f} \right) = -q_w$	$C = 0\%$
EA	$h = (H_s - y) \frac{\rho_s}{\rho_f}$	(1) $v \geq 0$ $\frac{\partial C}{\partial y} = 0$ (2) $v < 0$ $C = 100\%$
EF	$h = (H_s - y) \frac{\rho_s}{\rho_f}$	(1) $u \geq 0$ $\frac{\partial C}{\partial x} = 0$ (2) $u < 0$ $C = 100\%$

### 3. Results and Discussion

#### 3.1. Lab-Scale Experiments

At the end of Step 3, saltwater intrusion toward Well B exhibited varying behaviors owing to different pumping ratios (Figure 5). Table 5 shows the intrusion length, time to steady, and observation of upconing in Step 3. When the water pumping ratio was less than 1.2, the saltwater intrusion was not observed near Well B. When the ratio was within 1.2 to 1.9, the salt–freshwater interface curve moved right and upward without upconing to Well B. However, when the ratio was beyond 2.0, the upconing of saltwater into Well B was observed. In addition, the longest time was required to achieve the steady state at the ratios of 1.9 and 2.0, which indicates that the critical pumping ratio between the barrier and production wells was 1.9. To confirm whether the saltwater reached Well B with a pumping ratio of approximately 2.0, a secondary test was performed, and the results are shown in Figure 6. In this test, when the steady state of Step 3 was reached with a pumping ratio of 1.9, but without salinization of Well B, the pumping rate at Well B was increased so that the pumping ratio was equal to 2.3. As a result, the saltwater reached Well B after increasing the pumping ratio from 1.9 to 2.3. Therefore, within the frames of this experiment, the critical pumping ratio between the barrier and production wells was considered to be 1.9. Moreover, if the amount of water pumped from the production well did not exceed 1.9 times the amount of water pumped from the barrier well, the freshwater can be continuously pumped from the production well without salinization. Additionally, provided the pumpable amount of freshwater from the production well was determined by the pumping ratio, the pumped amount from the barrier well increased with that from the production well without risking production well salinization.

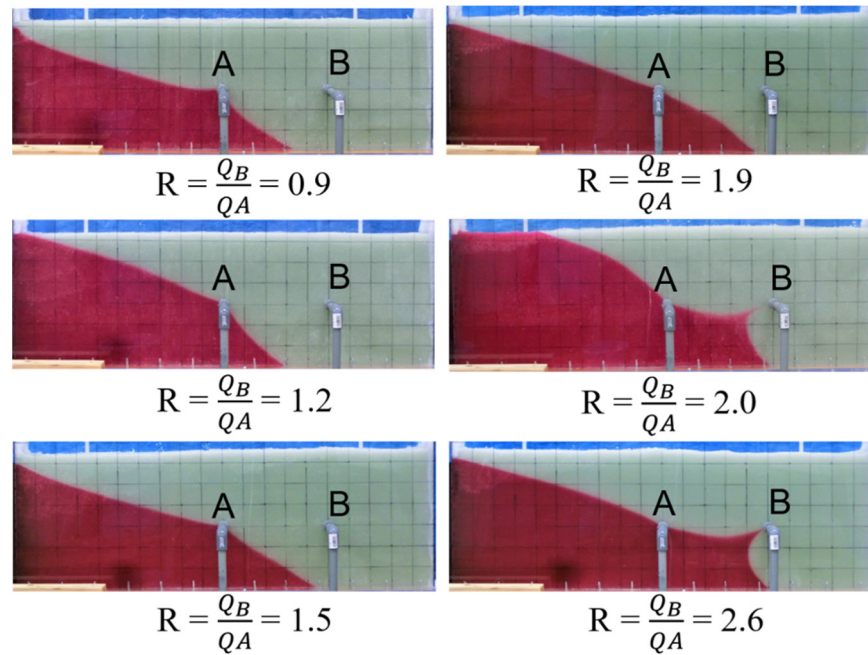


Figure 5. Results of experiments with the steady state at Step 3.

Table 5. Results for Step 3.

Intake Ratio; $Q_B/Q_A$	0.9	1.2	1.5	1.9	2.0	2.6
Intrusion length of saltwater (cm)	67.0	64.5	72.0	73.0	74.0	75.0
Time to reach steady state (min)	90	70	80	110	130	70
Upconing	×	×	×	×	○	○

(○ and × represent that upconing was observed and not observed, respectively, at the pumping ratio).

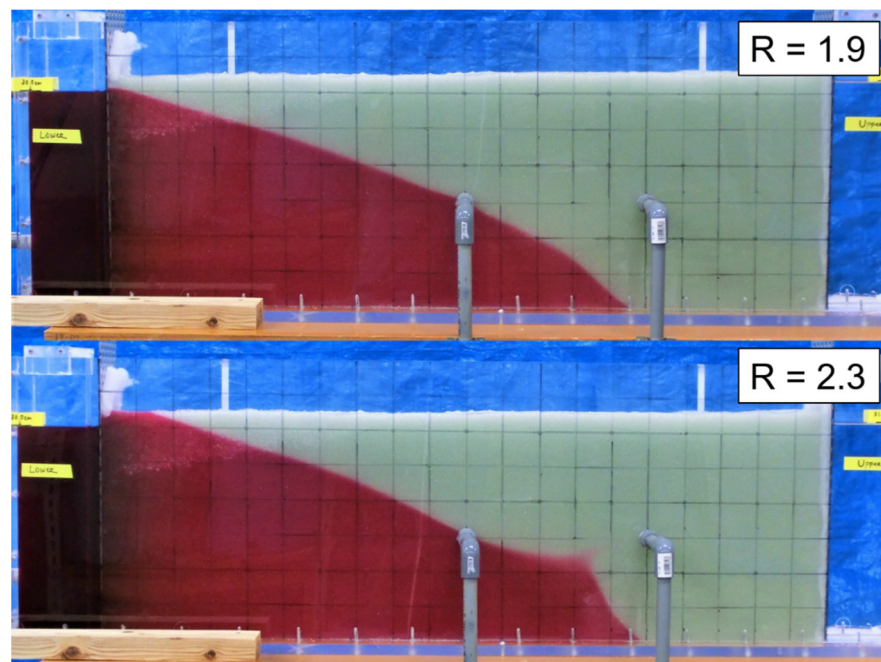


Figure 6. Result of the secondary test. Upconing was observed at  $R = 2.3$ , even though it was not observed at  $R = 1.9$ .

When pumping from Well B was stopped at Step 4, a retreat of the salt–freshwater interface was observed. Furthermore, even when the pumping ratio exceeded 1.9, with which Well B was salinized, the upconing toward Well B disappeared and the salt–freshwater interface retreated to its initial position. Figure 7 represents the change in saltwater intrusion length at its toe position over time from the end of Steps 2–4. The toe position of the saltwater moved to its initial position at the end of Step 4. Furthermore, comparing saltwater intrusion areas recorded at the end of Step 2 with those recorded at Step 4, the positions, shapes, and areas of saltwater in both steps were found to be almost identical, indicating that the salt–freshwater interface retreated to the same position before pumping from Well B started (Figure 8). Therefore, it is considered that despite the salinization of the production well, the barrier well has a positive effect on retreating the saltwater intrusion toward the previous state.

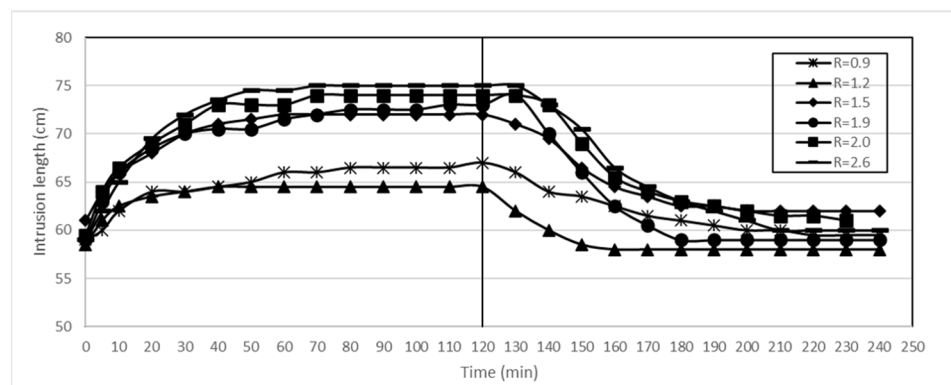


Figure 7. Change in intrusion lengths over time from the end of Step 2 to Step 4.

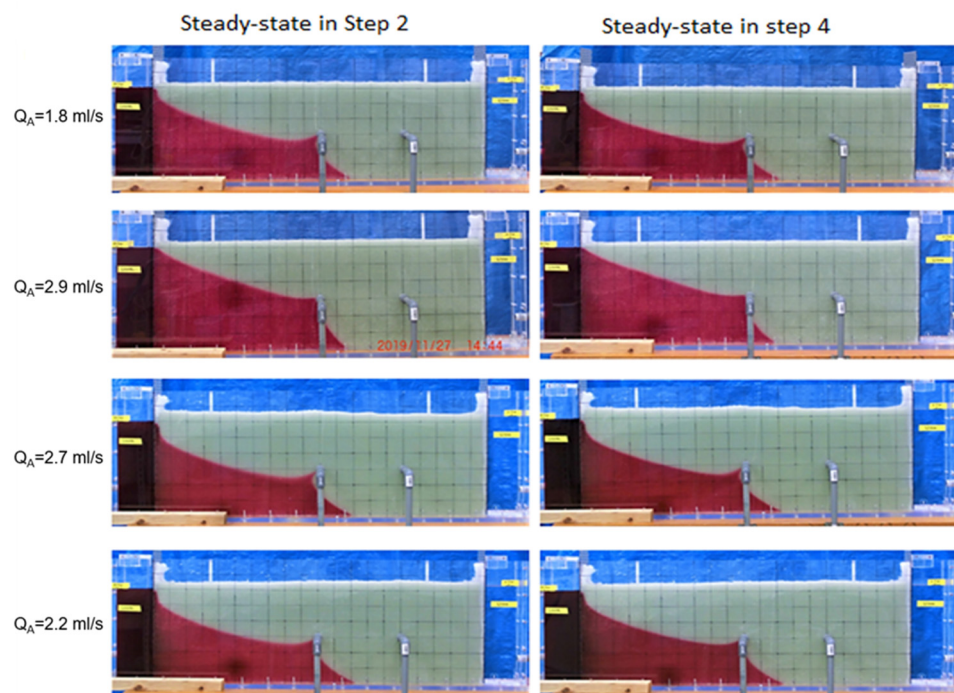
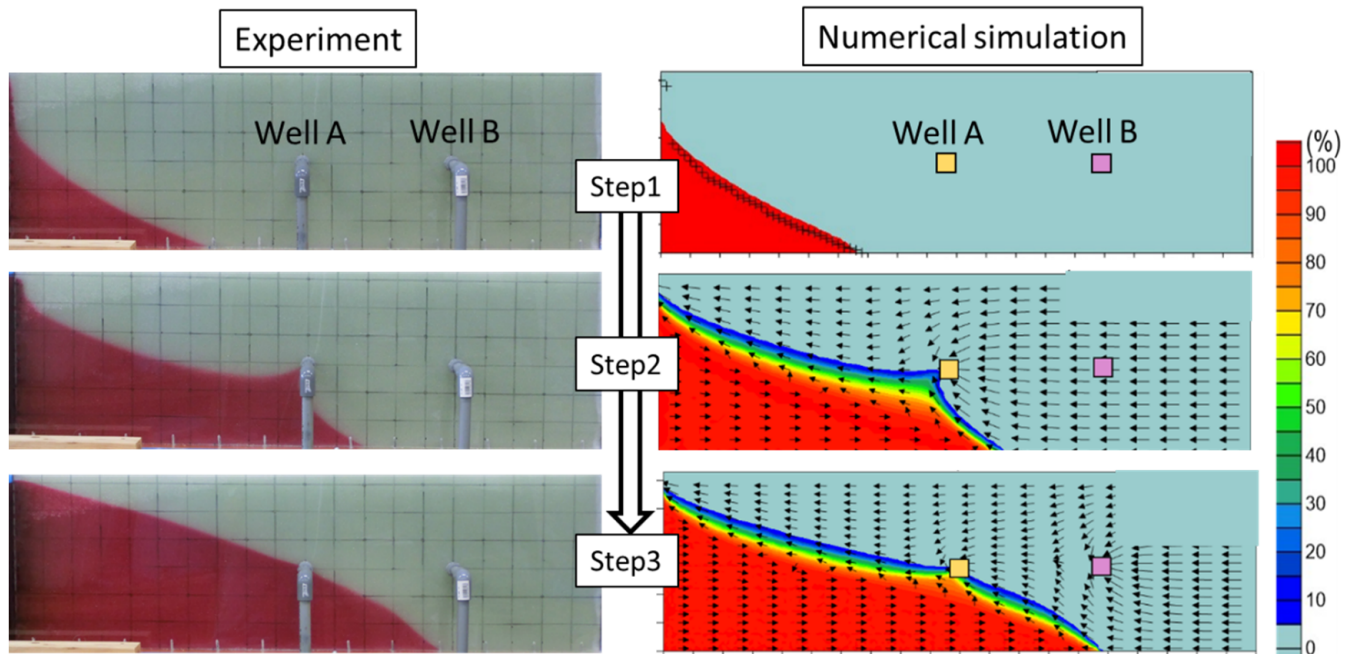


Figure 8. Comparison of steady states at the end of Steps 2 and 4.

### 3.2. Numerical Simulation

The experimental and numerical results were compared based on the general condition of the fresh-saltwater interface and the intrusion length at each steady state. The error in

the intrusion length was less than 2.5 cm in any cases, and the general shape of the fresh–saltwater interface was calculated with high accuracy. Figure 9 shows the experimental and numerical results in Step 1, 2, and 3 for  $R = 1.9$  as an example. As shown in the figure, the general shape of the interface was accurate and the error in the intrusion length was less than 1 cm in each step. Therefore, it was regarded that the numerical simulation was reliable in this study.



**Figure 9.** Experimental and numerical simulation results (steady states in each step) for  $R = 1.9$ .

From the numerical simulation, it was determined that there was water flow toward the barrier well when the barrier well was working (Figure 9). This freshwater flow transported saltwater from its toe at the bottom toward the barrier. This transportation can maintain the equilibrium between saltwater inflow and outflow at the steady state, preventing further saltwater intrusion, especially in front of the saltwater interface. This transportation of saltwater is related to the efficiency of saltwater extraction by the barrier well. Thus, it is considered that the high performance of the barrier well can be obtained when the freshwater flow toward the barrier well is larger than the saltwater flow. Furthermore, there was a trend that the concentration of extracted saltwater by the barrier increased when the pumping ratio was increased to the critical pumping ratio (Figure 10). Although the salinity level of upconing was low in the case of 0.9, upconing of highly concentrated saltwater was observed in the cases from 1.2 to 1.9. In contrast, when the pumping ratio was 2.3, the upconing of highly concentrated saltwater became smaller than that in the case of 1.9. Moreover, in the case of 2.6, upconing toward Well A completely disappeared, and the barrier well only extracted low-concentration saltwater. From these simulated results, it is considered that the effect of the barrier well on saltwater intrusion has four stages, as follows. In the first stage, in which the pumping ratio is significantly lower than the critical ratio, the barrier effectively prevents saltwater intrusion by extracting low-concentration saltwater. Although the barrier well does not extract highly concentrated saltwater at this stage, pumping from the barrier well forms the freshwater flow toward the barrier well, increasing the seaward flow and preventing the movement of saltwater. In the second stage, in which the pumping ratio is less than or equal to the critical ratio, the barrier well extracts highly concentrated saltwater, which prevents the movement of the high-concentration zone. The extraction of highly concentrated saltwater has a large impact on the prevention of saltwater intrusion because the saltwater flow of

highly concentrated saltwater dominates the saltwater flow due to the large difference in densities between saltwater and freshwater. In the third stage, in which the pumping ratio is slightly beyond the critical ratio, the extraction of highly concentrated saltwater toward the barrier decreases. Although the barrier well can extract highly concentrated saltwater, the influence of extraction decreases and it cannot prevent the movement of the high-concentration zone, which increases the mixing zone and the risk of salinization of the inland production well. In the final stage, in which the pumping ratio significantly exceeds the critical ratio, the barrier well extracts only low-concentration saltwater. The saltwater flow in the mixing zone is formed by pumping from the production well, and the barrier well cannot have positive effects on saltwater extraction, which indicates that the barrier well cannot prevent saltwater intrusion at this stage.

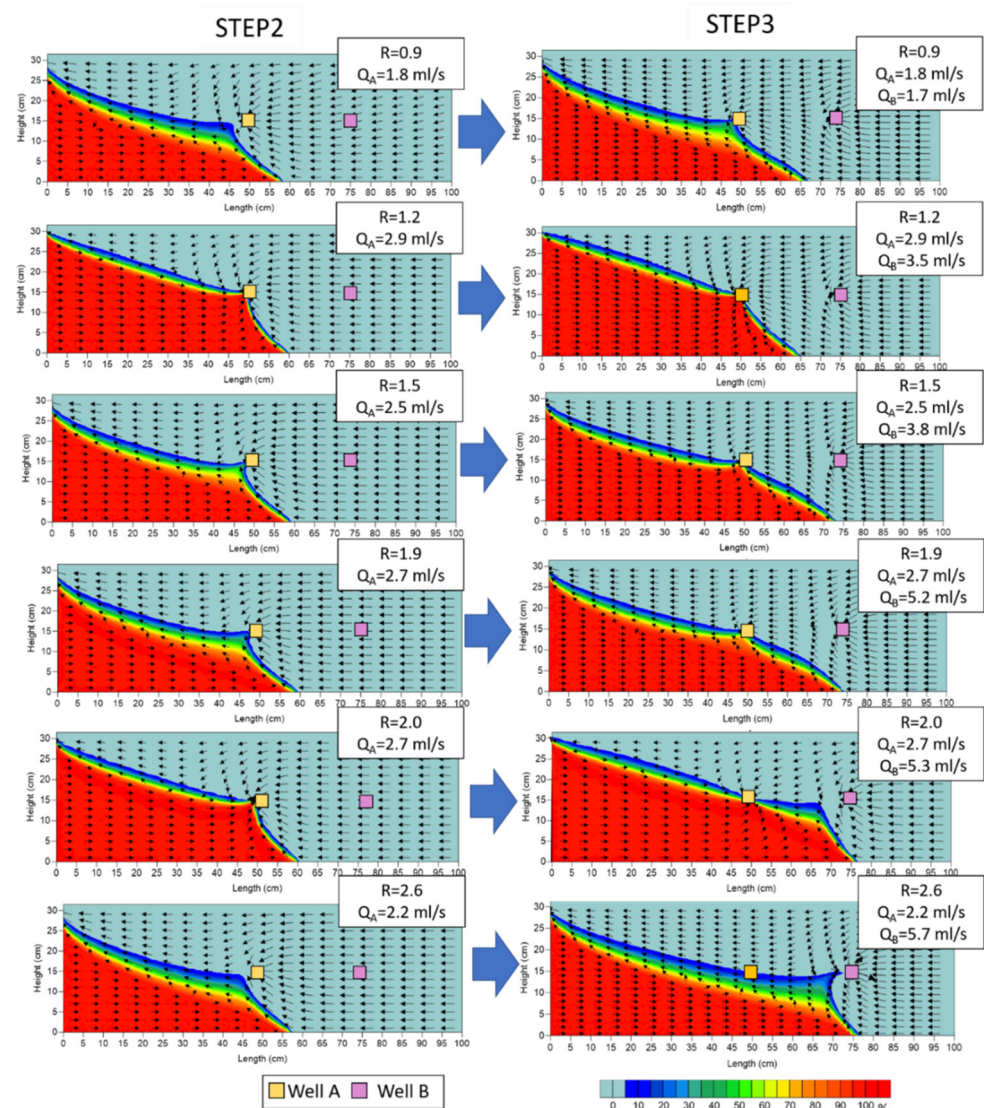


Figure 10. Comparison of steady states at Steps 2 and 3.

#### 4. Conclusions

This study tested the effectiveness of saltwater pumping from a barrier well on the possible flow rate from a production well by lab-scale experiments and two-dimensional numerical simulations. In lab-scale experiments, a lab-scale model simulating a sandy coastal unconfined aquifer was created to investigate the effect of different pumping ratios on the behavior of saltwater intrusion. It was revealed that there was a quantitative relationship in the pumping ratio between barrier and production wells, and the critical

pumping ratio between them was 1.9 under the experimental conditions. Moreover, the experiments showed that a barrier well can restore an aquifer to the previous state, despite the salinization at the production well, as compared in Steps 2 and 4. To analyze the experimental results, a numerical model based on the groundwater flow equation and solute transport equation was created and simulated under the same conditions as the experiments. From the numerical simulation, the mechanism of saltwater transportation from high- to low-salinity zones was revealed. This numerical model demonstrated that the barrier effectively prevented saltwater intrusion by extracting highly concentrated saltwater when the pumping ratio was less than the critical ratio, and the extraction of low-concentration saltwater will be enough to prevent saltwater intrusion when the pumping ratio is much lower than the critical pumping ratio, for example, as observed at a pumping ratio of 0.9. Even when the pumping ratio approaches the critical ratio, the barrier effectively extracts highly concentrated saltwater, which has a large positive effect on preventing further saltwater intrusion. In contrast, when the pumping ratio significantly exceeds the critical pumping ratio, the barrier well cannot work sufficiently, leading to further saltwater intrusion and salinization of the production well. These findings demonstrate that pumping saltwater from a barrier well can protect production wells as long as the pumping ratio is well controlled to be under the critical pumping ratio. However, further studies are required to confirm the influence of the positions and numbers of the barrier and production wells on the critical pumping ratio. Besides, a three-dimensional model is required to simulate the actual conditions of coastal aquifers. With these further studies, this approach controlling the pumping ratio can be applied to actual coastal aquifers to manage saltwater intrusion.

**Author Contributions:** Conceptualization, Y.H.; methodology, Y.H.; software, S.O.; validation, S.O. and T.N.; formal analysis, S.O. and T.N.; investigation, C.A.A.; resources, Y.H.; data curation, S.O.; writing—original draft preparation, C.A.A. and S.O.; writing—review and editing, S.O.; visualization, S.O. and T.N.; supervision, Y.H.; project administration, Y.H.; funding acquisition, Y.H. All authors have read and agreed to the published version of the manuscript.

**Funding:** This research received no external funding.

**Institutional Review Board Statement:** Not applicable.

**Informed Consent Statement:** Written informed consent has been obtained from the patient(s) to publish this paper.

**Data Availability Statement:** The data that support the findings of this study are available from the corresponding author upon reasonable request.

**Acknowledgments:** We would like to thank Hideto Oishi, a technical staff member of Kyushu University, who made the wonderful laboratory equipment for us.

**Conflicts of Interest:** The funders had no role in the design of the study; in the collection, analyses, or interpretation of data; in the writing of the manuscript, or in the decision to publish the results.

## References

1. Abd-Elhamid, H.F.; Javadi, A.A.; Qahman, K.M. Impact of over-pumping and sea level rise on seawater intrusion in Gaza aquifer (Palestine). *J. Water Clim. Chang.* **2015**, *6*, 891–902. [[CrossRef](#)]
2. Sherif, M.; Sefelnasr, A.; Javadi, A. Incorporating the concept of equivalent freshwater head in successive horizontal simulations of seawater intrusion in the Nile Delta aquifer, Egypt. *J. Hydrol.* **2012**, *464–465*, 186–198. [[CrossRef](#)]
3. Mazi, A. *Seawater Intrusion Risks and Controls for Safe Use of Coastal Groundwater under Multiple Change Pressures*; Department of Physical Geography and Quaternary Geology, Stockholm University: Stockholm, Sweden, 2014.
4. Ebeling, P.; Händel, F.; Walther, M. Potential of mixed hydraulic barriers to remediate seawater intrusion. *Sci. Total. Environ.* **2019**, *693*, 133478. [[CrossRef](#)] [[PubMed](#)]
5. Costall, A.; Harris, B.; Pigois, J.P. Electrical Resistivity Imaging and the Saline Water Interface in High-Quality Coastal Aquifers. *Surv. Geophys.* **2018**, *39*, 753–816. [[CrossRef](#)]
6. Werner, A.D.; Simmons, C.T. Impact of Sea-Level Rise on Sea Water Intrusion in Coastal Aquifers. *Ground Water* **2009**, *47*, 197–204. [[CrossRef](#)] [[PubMed](#)]

7. FAO (Food and Agriculture Organization). *Seawater Intrusion in Coastal Aquifers: Guidelines for Study, Monitoring, and Control*; FAO: Rome, Italy, 1997.
8. Sherif, M.M.; Singh, V.P. Effect of climate change on sea water intrusion in coastal aquifers. *Hydrol. Process.* **1999**, *13*, 1277–1287. [[CrossRef](#)]
9. IPCC. The Physical Science Basis. Contribution of Working Group I to the Fifth Assessment Report of the Intergovernmental Panel on Climate Change Stocker, T.F. Summary for policymakers. In *Climate Change*; Qin, D., Plattner, G.-K., Tignor, M., Allen, S.K., Boschung, J., Nauels, A., Xia, Y., Bex, V., Midgley, P.M., Eds.; Cambridge University Press: Cambridge, UK; New York, NY, USA, 2013; pp. 25–26. [[CrossRef](#)]
10. Hussain, M.S.; Abd-Elhamid, H.F.; Javadi, A.A.; Sherif, M.M. Management of Seawater Intrusion in Coastal Aquifers: A Review. *Water* **2019**, *11*, 2467. [[CrossRef](#)]
11. Stein, S.; Yechieli, Y.; Shalev, E.; Kasher, R.; Sivan, O. The effect of pumping saline groundwater for desalination on the fresh–saline water interface dynamics. *Water Res.* **2019**, *156*, 46–57. [[CrossRef](#)] [[PubMed](#)]
12. Vats, O.P.; Sharma, B.; Stamm, J.; Bhattacharjya, R.K. Groundwater Circulation Well for Controlling Saltwater Intrusion in Coastal aquifers: Numerical study with Experimental Validation. *Water Resour. Manag.* **2020**, *34*, 3551–3563. [[CrossRef](#)]
13. Sherif, M.M.; Hamza, K. Mitigation of Seawater Intrusion by Pumping Brackish Water. *Transp. Porous Media* **2001**, *43*, 29–44. [[CrossRef](#)]
14. Pool, M.; Carrera, J. Dynamics of negative hydraulic barriers to prevent seawater intrusion. *Hydrogeol. J.* **2009**, *18*, 95–105. [[CrossRef](#)]
15. Park, S.-U.; Kim, J.-M.; Yum, B.-W.; Yeh, G.-T. Three-Dimensional Numerical Simulation of Saltwater Extraction Schemes to Mitigate Seawater Intrusion due to Groundwater Pumping in a Coastal Aquifer System. *J. Hydrol. Eng.* **2012**, *17*, 10–22. [[CrossRef](#)]
16. Blair, T.C.; McPherson, J.G. Grain-size and textural classification of coarse sedimentary particles. *J. Sediment. Res.* **1999**, *69*, 6–19. [[CrossRef](#)]
17. Yu, C.; Cheng, J.; Jones, L.; Wang, Y.; Faillace, E.; Loureiro, C.; Chia, Y. *Data Collection Handbook to Support Modeling the Impacts of Radioactive Material in Soil*; U.S. Department of Energy Office of Scientific and Technical Information: Oak Ridge, TN, USA, 1993. [[CrossRef](#)]
18. Elizabeth, L.E.; Miguel, A.; Maria, G.; Eduardo, A. A model for calculating the density of aqueous multicomponent electrolyte solutions. *J. Chil. Chem. Soc.* **2008**, *53*, 1393–1398.
19. Simion, A.I.; Cristina, G.; Ana-Maria, R.; Lucian, G. Mathematical modelling of density and viscosity of NaCl aqueous solutions. *J. Agroaliment. Process. Technol.* **2015**, *21*, 41–52.
20. Castro-Orgaz, O. Steady free-surface flow in porous media: Generalized Dupuit–Fawer equations. *J. Hydraul. Res.* **2011**, *49*, 55–63. [[CrossRef](#)]
21. Jinno, K.; Momii, K.; Fujino, K.; Nakagawa, K.; Hosokawa, T.; Egusa, N.; Hiroshiro, Y. *Numerical Analysis of Mass Transport in Groundwater*; Kyushu University Press: Fukuoka, Japan, 2001; pp. 13–72. (In Japanese)
22. Van Genuchten, M.T. A closed-form equation for predicting the hydraulic conductivity of unsaturated soils. *Soil Sci. Soc. Am. J.* **1980**, *44*, 893–898. [[CrossRef](#)]
23. Jinno, K.; Momii, K.; Fujino, K.; Nakagawa, K.; Hosokawa, T.; Egusa, N.; Hiroshiro, Y. *Numerical Analysis of Mass Transport in Groundwater*; Kyushu University Press: Fukuoka, Japan, 2001; pp. 83–84. (In Japanese)
24. Diersch, H.-J.; Kolditz, O. Variable-density flow and transport in porous media: Approaches and challenges. *Adv. Water Resour.* **2002**, *25*, 899–944. [[CrossRef](#)]
25. Harleman, D.R.F.; Rumer, R.R. Longitudinal and lateral dispersion in an isotropic porous medium. *J. Fluid Mech.* **1963**, *16*, 385. [[CrossRef](#)]